İSTANBUL UNIVERSITY PRESS

Physics and Astronomy Reports
PAR 2023, 1 (1), 32–37
DOI: 10.26650/PAR.2023.00004

RESEARCH ARTICLE

Laser Spectroscopic Investigation of the Hyperfine Structure of Atomic Manganese in the Mid-infrared Wavelength Range

S. Kröger [1*], L. Windholz[2], and Gö. Başar[3]

[1]Hochschule für Technik und Wirtschaft Berlin, Fachbereich 1, Wilhelminenhofstr. 75A, D-12459 Berlin, Germany
[2]Institut für Experimentalphysik, Technische Universität Graz, Petersgasse 16, Graz A-8010, Austria
[3]Istanbul University, Faculty of Science, Department of Physics, TR-34134 Vezneciler, Istanbul, Turkiye

ABSTRACT

The hyperfine structure of atomic manganese was studied with laser induced fluorescence spectroscopy and optogalvanic spectroscopy using a commercial hollow cathode discharge lamp and a fully automated single mode mid-infrared tunable laser diode system in the wavelength range from 1530 nm to 1610 nm. Five spectral lines has been analysed. Magnetic dipole hyperfine structure constants A for seven levels were determined by fitting the hyperfine structure using Voigt profile functions. For two levels, the A constants were determined experimentally for the first time. For the other levels, the previously published hyperfine structure constants A could be confirmed and the accuracy of the values could be improved. When comparing our two new experimental A-constants with calculated A-constants from the literature, which originate from a semi-empirical analysis of the odd parity levels in Mn, large deviations were found. Until now, experimental values were missing for a more precise calculation. Our new values offer the possibility for a future optimisation of the calculation.

Keywords: laser spectroscopy – hyperfine structure – manganese

1. INTRODUCTION

Lasers in the visible and near infrared spectral range up to 1000 nm have been used very successfully for many decades for the investigation of atomic hyperfine structure (hfs) and isotopic shifts. For some time now, suitable laser light sources have also been available in the infrared spectral range above 1000 nm, but so far they have not been used for such applications. Presented here for the first time is the use of a fully automated diode laser system in the mid-infrared to measure the hfs of atomic transitions of manganese. The device used offered a fast and straightforward possibility to study atomic spectra at high resolution without using additional devices for characterizing the laser radiation, such as a wavemeter or a reference marker Fabry-Perot-Interferometer (see Section 2).

Manganese (Mn) with the atomic number 25 is one of the 3d elements and belongs to the elements with only one stable isotope. This isotope, ^{55}Mn, has a nuclear spin of $I = 5/2$ and a nuclear magnetic dipole moment of $\mu = 3,468716\,(2)\,\mu_N$ (Lederer & Shirley 1978), leading to a broad hfs splitting in Mn spectra. This splitting is also clearly seen in Doppler broadened spectra. The electric quadrupole moment with $Q = 0.33\,(1)$ barns (Lederer & Shirley 1978) causes only a small deviation of the magnetic dipole hfs, which is not well detectable at the resolution of our experiments.

In the last decades several investigations of the fine structure and hfs of atomic Mn have been conducted, see Lefèbvre et al. (2003); Başar et al. (2003); Blackwell-Whitehead et al. (2005); Acar et al. (2005); Klose et al. (2013); Głowacki et al. (2020a,b); Elantkowska et al. (2022); Głowacki et al. (2022) and references therein. Although much research has been done, there are still many gaps in the hfs data for Mn I and reliable laboratory data are an important prerequisite for the study of astrophysical spectra, for example for the analysis of stellar abundances and for the determination of physical parameters in stellar atmospheres.

Three of the five infrared Mn lines presented here have already been studied by Meléndez (1999) who fitted the solar spectrum. The resolution in our spectra is significantly better than in the solar spectrum. Meléndez has explicitly pointed out in his paper that laboratory measurements are necessary to improve the accuracy of HFS splitting.

Corresponding Author: S. Kröger **E-mail:** sophie.kroeger@htw-berlin.de
Submitted: 30.04.2023 • **Revision Requested:** 15.05.0023 • **Last Revision Received:** 19.05.2023 • **Accepted:** 22.05.2023 • **Published Online:** 30.05.2023

2. EXPERIMENTAL

Laser induced fluorescence spectroscopy (LIF) and optogalvanic spectroscopy (OGS) have been applied for the measurements of the hfs of Mn spectra. The experimental set up allowed to measure with both methods simultaneously.

The free Mn atoms were produced in a commercial hollow cathode lamp (Hamamatsu Photonics) with Ne as buffer gas. The discharge ran with a current of about 20 mA.

A single mode mid-infrared tunable laser diode system (DLC CTL 1550 from TOPTICA Photonics) with an optical power of about 40 mW in the wavelengths in the range from 1510 nm to 1630 nm was used to excite the Mn atoms. The laser was controlled fully automatically via the laser DLC controller. The wavelength could be mode-hop free tuned over the entire wavelength range. The scanning speed and step width could be adjusted. The laser controller has four integrated AD converters, two of which were used to measure for the LIF and OGS signals, respectively. Measurements are taken via the supplied DLC pro PC-GUI control software, which allows easy control of the laser and simultaneous measurement data acquisition.

The laser beam was amplitude-modulated by a mechanical chopper with a frequency of slightly below 3 kHz. The Lock-in technique was used to filter out the OGS and LIF signals from the corresponding signals. For OGS, the laser-induced change of the discharge voltage measured across a ballast resistor was sent to the lock-in amplifier. For LIF, the light from the plasma was coupled to a monochromator (McPherson with a grating with 1200 lines/mm) and detected with a photomultiplier (Hamamatsu R928). The signal from the photomultiplier was sent to a second lock-in amplifier in order to detect the change in intensity of the fluorescence caused by the laser light. The fluorescence light from the laser-induced transition was detected at a selected wavelength of the monochromator with a wavelength precision of 0.1 nm.

The laser diode system DLC CTL is able to scan the wavelength very quickly. Since the intensity of the investigated Mn lines was relatively weak compared to the neighboring noble gas (Ne) lines, a high time constant of 300 ms or 1 s had to be set at the lock-in in order to minimise noise and make the lines stand out clearly from the noise. The scanning speed had to be adapted to this time constant and therefore a slow scanning speed was chosen. Scan times of 0.02 nm per minute data and a step size of 0.0005 nm have been set on the laser controller.

The PC control software provides a cvs data file with the wavelength and the signal(s) of the AD converter(s). The OGS signal was always measured with the first AD converter. For three lines, the LIF signal was recorded additionally with the second AD converter. For two lines, no fluorescence line with a sufficiently strong LIF signal was available. These lines were only measured with OGS.

The absolute wavelengths given by the DLC CTL control are not calibrated. The investigated spectral lines could nevertheless be clearly assigned. The position of the lines was determined relative to the neighboring noble gas lines and the wavelengths were additionally checked with an external wavemeter (HighFinesse WS7-60). Since the determination of the absolute wavelength is not the focus of interest in this present work, no further effort was made at this point. In the following, the wavelength calculated from the level energies using the Rydberg-Ritz combination principle is used to mark the lines.

The temporal linearity of the laser scan was checked and confirmed with the external HighFinesse wavemeter, which ran parallel to the measurement but was recorded separately.

Despite the linearity of the wavelength change, the data increments of the measurement data are not exactly uniform. For the subsequent evaluation of the experimental data (see Section 3), equidistant data on a frequency axis are required. Therefore, the data of the experimental wavelengths in the measured spectra were converted into frequencies. Subsequently, the spectra consisting of frequency and intensity data pairs were transferred by linear interpolation to equidistant interpolation points with a step size of 40 or 50 MHz using a Python script. Each line was measured and analysed at least five times.

3. HYPERFINE STRUCTURE ANALYSIS

In the wavelength range of the laser system (from 1510 nm to 1630 nm), five Mn lines could be unambiguously classified. The classification of the lines was done with program *Elements* (Windholz & Guthöhrlein 2003; Windholz 2016), which used a list of levels of atomic and singly ionic Mn from **?** to search for transitions matching the wavelengths. Three of the lines are found in the literature and had already been classified by Meléndez (1999).

The lines are compiled in Table 1, sorted by lower level, and shown in Figures 1 and 2. The wavenumbers σ are the centre-of-gravity of the hfs calculated using the Rydberg-Ritz combination principle from the fine structure level energies. The wavelengths in air λ_{air} are calculated from the wavenumbers. The level energies values and J quantum numbers of the lower and the upper levels are given according to the database from Kurucz[1]. In the seventh column, the experimental method used is listed. In the final column, a comment concerning the hfs analysis is given.

For all lines, the lower level has even parity. Three and two lines, respectively, each have the same lower level. The three lines connected to the lower level 39 431.368 cm^{-1} (see Figure 1) were measured with OGS and LIF. For the LIF measurements in all three cases the same fluorescence line was used, $\lambda_{\mathrm{air,\,f}} = 482.35$ nm, starting from the lower level of the laser transition. The signal-to-noise ratio was slightly better using LIF than OGS. The measurement results of both spectroscopy

[1] http://kurucz.harvard.edu/atoms/

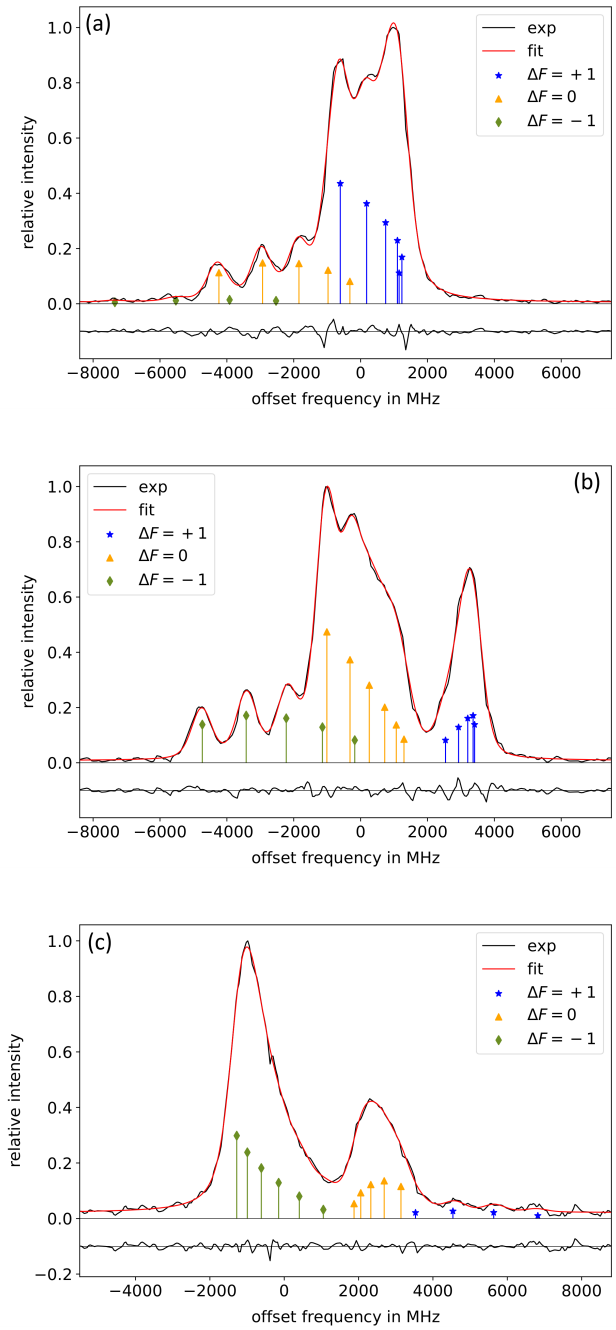

Figure 1. Hfs spectra of the three lines connected to the lower level 39 431.368 cm^{-1}, $J = 7/2$ recorded with LIF, together with the best fit curves. The hfs components are marked by the difference ΔF of the total angular momenta of the upper and lower hfs levels. In the lower part of each figure, the difference between experimental and best-fit curves is given. a) transition to upper level 46 026.238 cm^{-1}, $J = 9/2$, b) transition to upper level 46 000.874 cm^{-1}, $J = 7/2$, c) transition to upper level 45 981.621 cm^{-1}, $J = 5/2$.

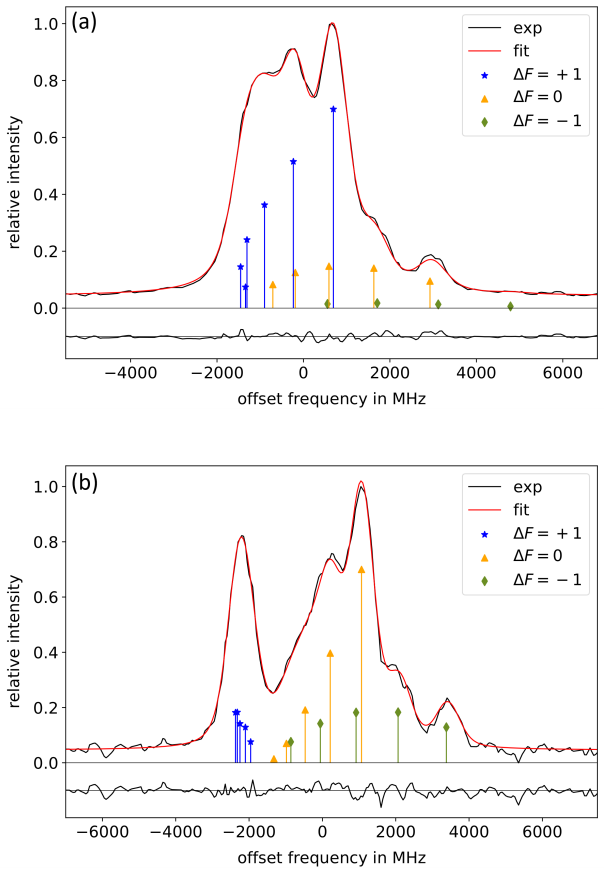

Figure 2. Hfs spectra of the two lines connected to the lower level 49 415.397 cm^{-1}, $J = 5/2$ recorded with OGS, together with the best fit curves. The hfs components are marked by the difference ΔF of the total angular momenta of the upper and lower hfs levels. In the lower part of each figure, the difference (diff.) between experimental and best-fit curves is given. a) transition to upper level 56 012.635 cm^{-1}, $J = 7/2$, b) transition to upper level 56 008.209 cm^{-1}, $J = 5/2$.

methods were used for the hfs analysis. As mentioned above, for the two lines, connected to the lower level 49 415.397 cm^{-1} (see Figure 2), no fluorescence line was found and therefore only OGS measurements are available for the hfs analysis.

To analyse hfs, the linearised experimental spectra were fitted with the computer program, Fitter (Zeiser et al. 2022). The fitting program uses a list of parameters, which can be set as free parameters, coupled with other parameters or can be set to a specific value if required. The list of parameters comprises the centre of gravity of the total hfs, the hfs constants A and B of the upper and the lower levels, two parameters to take into account the height and slope of the background, as well as the relative intensity and two profile parameters for each individual hfs component. We chose a Voigt profile as the line profile function, which requires two full widths at half maximum (FWHM) profile parameters per individual hfs component, each one to describe the Gaussian and the Lorentzian parts of the Voigt profile.

As can be seen in Figure 1 and 2, with the resolution achieved in our experiment all lines are partly unresolved. Therefore the number of free parameters in the fit had to be reduced considerably. For this purpose

- the electric quadrupole hfs constants B of both levels were set to be zero,
- for three lines the magnetic dipole hfs constants A of the lower level was fixed (see Table 1),
- the Gaussian part of the Voigt profile is set to be equal for all hfs components,
- the Lorentzian part of the Voigt profile is set to be equal for all strong hfs components with $\Delta F = \Delta J$ and for all weak hfs components with $\Delta F \neq \Delta J$, and
- the intensities of the individual hfs components are coupled to each other.

The explanation for these steps is given in the following paragraphs.

The hfs constants B were set to zero because the influence of the electric quadrupole interaction is very small for Mn (as mentioned in the introduction) and it was not possible to determine reliable values for the B constants with our Doppler-limited spectra.

To determine the A value of the lower levels, in each set of lines connecting the same lower level the best resolved line was selected. This line was fitted with magnetic dipole hfs constants A of the lower level and the upper levels as freely floating parameters. The resulting A values were preset and fixed when fitting the hfs of the other lines. The corresponding information is given in the last column of Table 1.

All lines are influenced by saturation effects, leading to a reduction in intensity as well as a broadening of the strong hfs components. As a consequence, the intensity ratios of the individual hfs components do not agree with the theoretical intensity ratios for electrical dipole transitions and the Lorentzian part of the full width at half maximum (FWHM) differs for different hfs components. For unsaturated spectra, all hfs components could have been fitted with the same Voigt FWHM. For saturated spectra, the Gaussian parts of the Voigt profile remains only slightly affected by saturation, whereas the width of the Lorentzian contribution varies. To account the saturation broadening of the strong hfs components in our spectra, two parameters for the Lorentzian part were fitted as freely floating parameter, one for all strong hfs components with $\Delta F = \Delta J$ and one for all weak hfs components with $\Delta F \neq \Delta J$.

To account for the saturation of the intensities of all hfs components, a single parameter was applied. Based on this parameter, theoretical values were calculated for the saturated intensities of the individual hfs components. These values were then used to couple to the intensity ratios during the fit. This method was presented in previous papers by one of the authors (LW) (Sobolewski 2019, 2020; Faisal 2020). The saturation parameter is not implemented in the fit program, therefore the parameter was changed step by step by hand until the optimal fit with minimised sum of squares of the residuals was found.

The saturation effects were much stronger for the lines connected to the lower level 39 431.368 cm^{-1} than for the lines connected to the lower level 49 415.397 cm^{-1}. The saturation-induced intensity increase of the weak components relative to the strongest component was between 2.5 and 3.0 for the lines connected to the lower level 39 431.368 cm^{-1}, while it was only 1.4 for the other lines.

The FWHM of the Voigt profiles was for all lines in the order of magnitude of 700 to 800 MHz and the FWHM of the Gaussian parts in the order of magnitude of 530 MHz to 600 MHz. Depending on the different lines the FWHM of the Lorentzian parts varied between 200 MHz to 440 MHz.

The resulting magnetic dipole hfs constants A_{exp} are listed in Table 2 together with the values from the literature, if available. The term designation according to (Elantkowska et al. 2022; Głowacki et al. 2022) is given in the fourth column. The spectral lines used for the determination of the A constants are indicated in the fifth column.

The reported constants A_{exp} are the mean values of the fit results of all measurements of the respective line. The uncertainties, indicated within brackets, consider both the standard deviation associated with the mean value and the error bar of the fixed A value, assuming the A constant of the lower level had been fixed during the fit.

For five levels, our A constants are in good agreement with the values from the literature (Brodzinski et al. 1987; Blackwell-Whitehead et al. 2005). The accuracy of the A constants could be improved.

For comparison, in the last two columns from Table 2 calculated values for the A constants, resulting from semi-empirical analysis of the odd and even parity level system in Mn (Elantkowska et al. 2022; Głowacki et al. 2022) are given. The calculated values from the literature for the two even parity levels show a very good consistency with the experimental A constants, much better than for the odd parity levels. For the levels with odd parity, a deviation in the order of 60 to 100 MHz can be seen for the levels whose A constants were already known previously and were taken into account in the semi-empirical calculation. For the two levels with previously unknown A-constants, the deviation of our experimental values A_{exp} from the predicted constants A_{calc} from the semi-empirical fit lies at 280 MHz and 380 MHz and is much larger. This emphasises the importance of our experimental results. The enlargement of the experimental database will lead to an improvement in the results of semi-empirical calculations if the new values will be taken into account.

4. CONCLUSION AND OUTLOOK

For the first time, a laser system in the mid-infrared spectral range was used to investigate the hfs in atomic spectra. Due to the implementation of a fully automated controller, the measurements could be carried out quickly and easily. The hfs of five spectral lines of atomic Mn has been investigated. Magnetic dipole hfs constants A for seven levels were obtained, two

Table 1. Lines of atomic manganese measured with LIF or OGS.

Line		Even level		Odd level			
λ_{air} (nm)	$\tilde{\nu}$ (cm^{-1})	E_e (cm^{-1})	J_e	E_o (cm^{-1})	J_o	Method	Comment
1 515.916	6 594.870	39 431.368	7/2	46 026.238	9/2	LIF	A_{lower} fixed during the fit
1 521.769	6 569.506	39 431.368	7/2	46 000.874	7/2	LIF	Both A constants fitted independently
1 526.242	6 550.253	39 431.368	7/2	45 981.621	5/2	LIF	A_{lower} fixed during the fit
1 515.372	6 597.238	49 415.397	5/2	56 012.635	7/2	OGS	A_{lower} fixed during the fit
1 516.389	6 592.812	49 415.397	5/2	56 008.209	5/2	OGS	Both A constants fitted independently

Table 2. Experimental magnetic dipole hyperfine structure constants A (in MHz) for levels of atomic manganese (sorted by parity p).

E (cm^{-1})	J	p	Config., term [3,4]	λ (nm)	A_{exp}	A_{ef}	Reference	A_{calc}	Reference
39 431.368	7/2	e	$3d^5(^6S)4s5s\ ^8S$	1521 .769	736.2 (15)	737 (3)	[1]	738	[3]
49 415.397	5/2	e	$3d^5(^6S)4s5s\ ^6S$	1516 .389	-632 (4)	-642 (9)	[1]	-682	[3]
45 981.621	5/2	o	$3d^5(^6S)4s5p\ ^8P$	1526 .242*	826.3 (21)	824 (3)	[2]	719	[4]
46 000.874	7/2	o	$3d^5(^6S)4s5p\ ^8P$	1521 .769	620.0 (11)	621 (3)	[2]	555	[4]
46 026.238	9/2	o	$3d^5(^6S)4s5p\ ^8P$	1515 .916*	518.6 (19)	519 (3)	[2]	467	[4]
56 008.209	5/2	o	$3d^5(^6S)4s8p\ ^6P$	1516 .389	-470 (6)			-82	[4]
56 012.635	7/2	o	$3d^5(^6S)4s5p\ ^6P$	1515 .372*	-372 (7)			-92	[4]

(*): hfs constants A of the lower level were fixed during the fit.

[1]: Brodzinski et al. (1987), [2]: Blackwell-Whitehead et al. (2005), [3]: Elantkowska et al. (2022), [4]: Głowacki et al. (2022)
Note: values from Brodzinski et al. (1987) and Blackwell-Whitehead et al. (2005) have been converted to MHz from mK = 10^{-3} cm^{-1}.

of these for the first time. Our newly obtained A constant values exhibit concurrence with the values characterized by previously established literature and are within the designated error limits, wherein our values have less errors. The two new A constants point out a large discrepancy between the experimental values and predicted literature values resulting from a semi-empirical analysis (Głowacki et al. 2022). We recommend that the calculation should be repeated with our new values.

In the Mn spectrum between 1510 nm to 1630 nm, there were a few more Mn lines that could not be classified. This means that at least one of the two levels involved must be unknown for each line. We will try to solve the problem of these unclassified lines as well. For this, however, further experiments must be carried out.

Peer Review: Externally peer-reviewed.

Author Contribution: Conception/Design of study - S.K., Gö. B.; Data Acquisition - S.K.; Data Analysis/Interpretation - L.W., Gö. B., S.K.; Drafting Manuscript - S.K.; Critical Revision of Manuscript - Gö.B., L.W.; Final Approval and Accountability - S.K., Gö.B.

Conflict of Interest: Authors declared no conflict of interest.

Financial Disclosure: Authors declared no financial support.

ACKNOWLEDGEMENTS

Sophie Kröger acknowledges TOPTICA Photonics for loaning the laser system DLC CTL 1550 for the period of the measurements.

LIST OF AUTHOR ORCIDS

S. Kröger https://orcid.org/0000-0003-4991-9176
L. Windholz https://orcid.org/0000-0001-6078-6154
Gö. Başar https://orcid.org/0000-0002-2428-8163

REFERENCES

Acar G., Başar Gü., Başar Gö., Öztürk I. K., Kröger S., 2005, PhyS, 71, 245

Başar Gü., Başar Gö., Acar G., Öztürk I. K., Kröger S., 2003, PhyS, 67, 476

Blackwell-Whitehead R., Pickering J., Pearse O., 2005, ApJS, 157, 402

Brodzinski T., Kronfeldt H.D., Kropp J.R., Winkler R., 1987, ZPhyD, 7, 161

Elantkowska M., Ruczkowski J., Głowacki P., Stefańska D., 2022, JQSRT, 292, 108347

Faisal M., Windholz L., Kröger S., 2020, JQSRT, 245, 106873

Głowacki P., Stefańska D., Ruczkowski J., Elantkowska M., 2020a, JQSRT, 253, 107138

Głowacki P., Stefańska D., Elantkowska M., Ruczkowski J., 2020b, JQSRT, 249, 107013

Głowacki P., Stefańska D., Ruczkowski J., Elantkowska M., Chomski M., Furmann B., 2022, JQSRT, 287, 108245

Klose A., Minamisono K., Mantica P.F., 2013, PhRvA, 88, 042701

Lederer C.M., Shirley V.S., 1978, Tables of Isotopes, 7th ed.; Wiley: New York, US

Lefèbvre P.-H., Garnir H.-P., Biémont E., 2003, A&A, 404, 1153

Meléndez J., 1999, MNRAS, 307, 197

Sobolewski Ł.M., Windholz L., Kwela J., Drozdowski R., 2019, JQSRT, 237, 106639

Sobolewski Ł.M., Windholz L., Kwela J., 2020, JQSRT, 242, 106769

Windholz, L., Guthöhrlein G.H., 2003, PhST, 105, 55

Windholz, L., 2016, PhyS, 91, 114003

Zeiser A., Kröger S., Pooyan-Weis L., Windholz L., Guthöhrlein G., 2022, JQSRT, 290, 108294